Size of microvesicles from charged surfactant bilayers: Neutron scattering data compared to an electrostatic model

J. Oberdisse and G. Porte
Groupe de Dynamique des Phases Condensées, UMR 5581 du CNRS, Université Montpellier II, Case Courier 26, Place Eugène Bataillon, 34095 Montpellier Cedex 05, France
(Received 10 February 1997)

Electrostatic interactions can have a decisive influence on the shape and size of supramolecular aggregates. Recently, we reported on a study of the curvature instability of charged surfactant membranes. At high dilution (volume fraction less than 2 or 3%), microvesicles with a radius of less than 100 Å were found at thermal equilibrium. In the experimental section of this paper, we present a detailed investigation of the size of these vesicles as a function of charge, concentration, and salinity again using small angle neutron scattering. In the theoretical section, we propose a quantitative electrostatic cell model, which predicts vesicle sizes in good agreement with experiment. It is based on a numerical solution of the Poisson-Boltzmann equation, which allows the area densities of amphiphilic ions to equilibrate between the inner and outer monolayers of the vesicles, and the counterions to exchange from the inside to the outside of the vesicle.
[S1063-651X(97)11108-4]

PACS number(s): 82.70.Dd, 61.12.−q, 82.65.Dp

INTRODUCTION

In recent years several theoretical investigations [1–10] have been reported dealing with the bending elasticity of charged surfactant bilayers. Bilayers built up from identical monolayers stuck opposite to one another in a symmetrical manner have zero spontaneous curvature, so that their bending elasticity is written according to Helfrich [11]

$$dE=[\tfrac{1}{2}\kappa(c_1+c_2)^2+\overline{\kappa}c_1c_2]dA, \qquad (1)$$

where dE is the free energy spent to bend an area element dA of a membrane with the principle local curvatures c_1 and c_2. κ and $\overline{\kappa}$ represent, respectively, the mean and Gaussian curvatures rigidity moduli of the bilayer. For charged bilayers each bending modulus bears two contributions. The first one, the intrinsic bending elasticity, arises from the packing requirements of the surfactant molecules within the bilayer: it would be present even in the absence of charges. The second one is a specific effect of charges and corresponds to the free energy involved upon bending the electrostatic double layers. It can be expressed in terms of the electrostatic contributions κ_{elec} and $\overline{\kappa}_{\mathrm{elec}}$ to the total mean and Gaussian curvature rigidity moduli κ and $\overline{\kappa}$. The above theoretical calculations predict that κ_{elec} is always positive, whereas in some cases $\overline{\kappa}_{\mathrm{elec}}$ is negative. At sufficient area charge density for the bilayer and at low salt content in the aqueous solvent, the negative contribution of $\overline{\kappa}_{\mathrm{elec}}$ can become comparable to the positive contribution of κ_{elec} and entropically stabilized (polydisperse) vesicles can be formed. At even higher charge densities, the softening effect of $\overline{\kappa}_{\mathrm{elec}}$ dominates the positive stiffening of κ_{elec}, and one expects the flat bilayer to become unstable against spontaneous bending, leading to the formation of thermodynamically stable, presumably very small vesicles.

A number of interesting experimental evidences of the formation of vesicles, or ''onions'' (multilamellar vesicles), have been reported for different surfactant systems [12–23], some of them forming charged bilayers. The system studied by Kaler and co-workers [18–20] consists of mixed anionic and cationic surfactants in pure water: vesicles actually form when the composition in oppositely charged species deviates significantly from stoichiometry, so that the bilayers bear a finite area charge density. In the experimental work of Hoffman and co-workers [12–14], the regular lamellar phase of a nonionic surfactant system is charged by the addition of small amounts of an ionic surfactant, and again spontaneous bending is observed, revealed by the formation of multilamellar ''onionlike'' structures. We ourselves investigated a similar system made of initially neutral bilayers charged by a small proportion of an ionic amphiphile [23]: besides the onionlike structure which occurs at moderate surfactant concentration, we found in the very dilute range (typically below 2 or 3% volume fraction) solutions of thermodynamically stable single wall microvesicles with a radius below 100 Å. So, all these experimental facts nicely meet the theoretical expectation that charges induce bending of bilayers (especially Refs. [1] and [2]).

However, up to now theories are usually worked out in the form of a perturbative expansion of the free energy of the bilayer in the limit of local curvatures small compared to the inverse of the Debye screening length λ_d^{-1}. In this respect, they are indeed reliable to predict the onset of the spontaneous bending. But once the process has started, they cannot evaluate at what equilibrium curvature it will end up. This limitation is specially dramatic in the case of the system mentioned above where—in the absence of added salt—the microvesicles have very small radii. They exist only in a very limited range of the phase diagram and are unstable with respect to small additions of electrolyte ($>5\times10^{-4}$ M NaCl). The purpose of the present work is to investigate this situation in more detail.

Our work is organized in two parts. In the experimental part, we again use neutron scattering to characterize the

structure of the microvesicles in the dilute range of our former system. In addition to the classical form factor of hollow shells, including the size polydispersity, the intervesicle structure factor is now incorporated into the data treatment following the Hayter-Penfold procedure with the renormalization of Hansen and Hayter [the rescaled mean spherical approximation (RMSA)] [24]. We are thus able to measure with high precision the mean radius and the polydispersity in size of the microvesicles as function of the area charge density, the solvent salinity, and the total amphiphile concentration. In the theoretical part, we interpret these evolutions quantitatively in terms of a simple model accounting for the free energy of the counterion cloud around the vesicle. The model has the same basic structure as the ones used by others [25,26]. The charge distribution is calculated numerically within a cell model according to the (nonlinearized) Poisson-Boltzmann (PB) equation, similar to the one proposed in Ref. [27]. We explicitly allow for different ionic concentrations inside and outside the vesicle and different area charge densities for the inner and outer monolayers, which implies that the ions are able to leak trough the amphiphilic membrane. The only adjustable parameter is the effective intrinsic bending elasticity $\tilde{\kappa}_{\mathrm{eff}}(=\kappa+\overline{\kappa/2})$ of the neutral bilayer, which is found to be in the expected range of some k_BT. We show that such a model, which treats microscopic details such as hydrocarbon packing constraints or polar head interactions only through one effective bending constant, is capable of reproducing general phase behavior and vesicle parameters surprisingly well.

EXPERIMENTAL SECTION

As in [23], we start with the electrically neutral system: Triton X-100 is the nonionic surfactant and octanol is the neutral cosurfactant. A regular lamellar phase is obtained in the absence of an ionic additive over a very large range of dilution in pure water, provided that Ω, the cosurfactant to surfactant ratio, is set in the appropriate range: $0.35<\Omega<0.5$ in weight fraction. The ionic additive used is cetylpyridinium chloride (CPCl). Its relative amount Γ is defined in weight fraction as: $\Gamma=[\mathrm{CPCl}]/([\mathrm{CPCl}]+[\mathrm{TX100}]+[\mathrm{Oct}])$. The total concentration ϕ of amphiphile in weight fraction is $\phi=([\mathrm{CPCl}]+[\mathrm{TX100}]+[\mathrm{Oct}])/[\text{total sample mass}]$.

Triton X-100 is purchased from Labosi: it is the technical grade product manufactured by Union Carbide and we used it with no further purification. This surfactant of great industrial interest cannot be considered as a pure chemical compound: in particular, there is some polydispersity in the polyoxyethylene chain length distribution around the average of 9.5. In order to preserve mutual consistency between different samples, all solutions were made from the same TX100 batch. Octanol is purchased from Carlo Erba ''Analyticals'' grade and used as received. Water is first doubly distilled and then further deionized using standard ion exchange resins down to a conductivity of less than 10^{-1} μSiemens/cm. A 5% solution of TX100 exhibits about the same electrical conductivity as a 5×10^{-4} M KCl solution: in order to eliminate the free ions, the surfactant is first dissolved in water and the solution obtained deionized with an ion exchange resin. Special attention is paid to a possible adsorption of TX100 to the ion exchange resin, which is found to be less than 2% in all cases. Octanol is not expected to bring in charges, which we confirmed by conductivity measurements. The ionic surfactant used as the additive is cetylpyridinium chloride (CPCl) purchased from Fluka (purum grade) and purified along several recrystallizations from an ethanol-acetone mixtures.

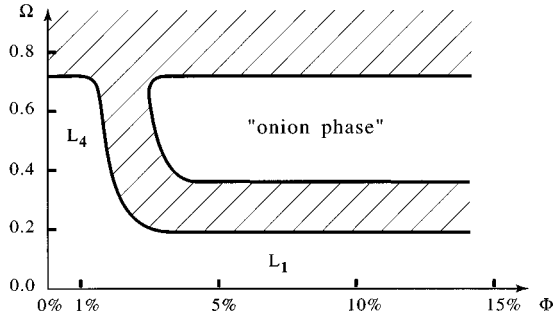

FIG. 1. Dilute part of the phase diagram of the system TX100/octanol/CPCl/H_2O.

A. Phase behavior

In Fig. 1, we show the phase diagram first reported in [23]. The horizontal axis corresponds to the total amphiphile concentration Φ and the vertical axis to the cosurfactant to surfactant ratio Ω. This section of the total phase behavior is taken at a fixed temperature ($T=20\,^{\circ}\mathrm{C}$), atmospheric pressure, and fixed relative amount of CPCl ($\Gamma=3.55\%$). In the high Ω range (between 0.4 and 0.8), where bilayers are stable, we find two distinct phases: at moderate dilution ($\phi>3$ or 4%), onionlike multilayered objects are stable making the phase very viscoelastic; at high dilution ($\phi<2$ or 3% typically) a very fluid dispersion of vesicles is found which we denote L_4: it is continuously connected to the regular micellar phase L_1 at lower Ω. In the following sections, we investigate in detail the microscopic structure of this dilute vesicle phase.

B. Neutron scattering

All neutron scattering data are collected on line PACE at the Laboratoire Leon Brillouin in Saclay. For all samples, D_2O is used as the aqueous solvent for obvious contrast reasons. A typical scattering pattern obtained in the dilute vesicle phase is shown in Figs. 2 and 3 (full circles). The composition of the corresponding sample is $\Phi=1\%$, $\Omega=0.5$, and $\Gamma=4\%$.

The purpose of our work is to investigate the interplay of charge and structure in the case of the microvesicles. We therefore concentrate on the determination of the characteristics of the vesicle phase—mean radius and size polydispersity—as a function of the charge Γ, the salinity of the aqueous solvent, and the total concentration in amphiphile. All scattering data, such as those of Fig. 2, are analyzed by modeling the scattered intensity in terms of the form factor of the individual vesicles in combination with the structure factor accounting for the spatial distribution of their center of mass.

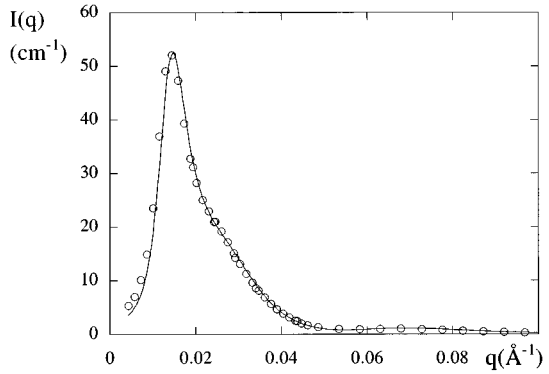

FIG. 2. Scattered intensity $I(q)$ for the sample $\Phi=1\%$, $\Omega=0.5$, $\Gamma=4\%$ (full circles), compared to a fit (full line) according to Eqs. (6), (7), and (8).

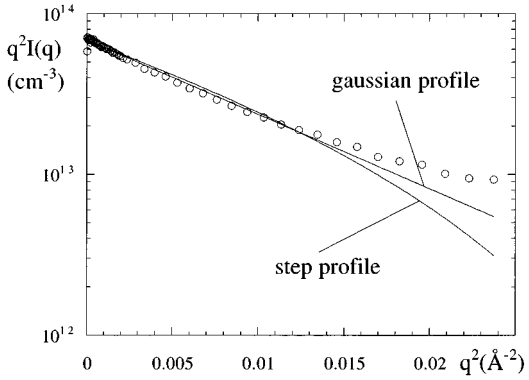

FIG. 4. Scattered intensity in the Guinier representation $q^2I(q)$ for the sample $\Phi=1\%$, $\Omega=0.5$, $\Gamma=0$ (full circles). Full lines are fits according to Eqs. (3a) and (3b).

1. Form factor

We expect the scattering patterns to reveal aggregates having the form of small vesicles. Due to the unknown degree of hydration of the oxyethylene head groups, the profile of the scattering length density across the bilayer is most probably not a rectangular single step: we rather expect it to be maximum inside the dry hydrophobic core and to decrease smoothly through the layers of hydrated head groups. A first plausible description of the contrast profile $\Delta\rho$ across the bilayer is a Gaussian function of width 2Δ.

$$\Delta\rho=\Delta\rho_m\exp\left(-\frac{z^2}{2\Delta^2}\right), \tag{2}$$

where z is the coordinate normal to the bilayer. A dilute lamellar sample consisting of such diffuse (Gaussian) layers would scatter according to

$$I(q)=2\pi\Phi V_A\,\frac{\Delta\rho_m^2}{q^2}\exp(-q^2\Delta^2), \tag{3a}$$

where $\Delta\rho_m$ is the maximum contrast in the middle of the bilayer in cm/cm^3, V_A is the bilayer volume per unit area, and Φ the surfactant volume fraction. On the other hand, the scattered intensity in the case of a rectangular single step profile of width δ and average contrast across the bilayer $\Delta\rho_a$ would be

$$I(q)=4\pi\,\frac{\Phi}{\delta}\,\Delta\rho_a^2\,\frac{[1-\cos(q\delta)]}{q^4}. \tag{3b}$$

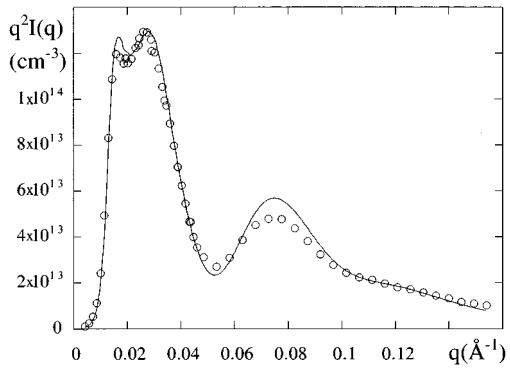

FIG. 3. Scattered intensity (full circles) and fit (full line) in the Guinier representation $q^2I(q)$ appropriate for bilayers for the sample $\Phi=1\%$, $\Omega=0.5$, $\Gamma=4\%$.

In order to characterize the bilayers quantitatively, we first collected the scattering pattern of a very dilute ($\Phi=1\%$, $\Omega=0.5$, $\Gamma=0.$, see full circles in Fig. 4) lamellar sample of the neutral system. A fit using expression (3a) yields $2\Delta=20$ Å and $\Delta\rho_m=6\times10^{10}$ cm^{-2}, whereas expression (3b) gives $\delta=33$ Å and $\Delta\rho_a=5.4\times10^{10}$ cm^{-2}, which is comparable to the dry layer thickness $\Delta_{\rm dry}=\Phi(2\pi/q_0)=30$ Å determined from the position q_0 of the Bragg peak as a function of concentration Φ. The $\Delta\rho$ values are typical for aliphatic chains in heavy water. Neither one of the two models is completely satisfactory in the high q range, but further refinements of the model profile would be physically not very meaningful. All form factor fits rely on these values for the contrast ($\Delta\rho_m$ or $\Delta\rho_a$) and the bilayer width (Δ or δ). The form factor of a vesicle made of a Gaussian bilayer of width 2Δ and of mean radius R can be calculated according to [28]

$$P^{\rm ves}_{\rm Gauss}(R,q)=32\pi^3\Delta\rho_m^2\exp(-q^2\Delta^2)\left[\cos(qR)\Delta^3+R\,\frac{\Delta}{q}\sin(qR)\right]^2, \tag{4}$$

whereas the form factor calculated with a rectangular single step of width $\delta=R_o-R_i$, mean radius $R=(R_o+R_i)/2$, in vesicular geometry is given by

$$P^{\rm ves}_{\rm step}(R,q)=\frac{16\pi^2\Delta\rho_a^2}{q^6}\,[\sin(qR_i)-qR_i\cos(qR_i)-\sin(qR_o)+qR_o\cos(qR_o)]^2, \tag{5}$$

where R_i and R_o are the inner and outer radius, respectively.

2. Structure factor

The physical situation corresponds to a gas of charged objects surrounded only by their counterions and therefore strongly interacting over large distances. The conductivity of the neutral sample, about 1 μS/cm, corresponds to a Debye screening length λ_d of the order of thousands of Å. Electrostatic interactions therefore induce strong local correlations, which manifest themselves in the strong maximum visible in the scattered intensity $I(q)$, see Fig. 2.

A satisfactory description can be obtained using the analytical structure factor calculated by Hayter and Penfold, with the high charge renormalization of Hansen and Hayter [24]. Special attention has to be paid to the fact that the vesicles are filled with solvent. Such a model structure factor makes use of a Debye-Hückel description of the vesicle-interaction potential. In the absence of salt, and the electric surface potentials being very high, the use of this structure factor will supply us with effective values only for the charge area density and for the screening length λ_d. We therefore enforce an effective value for the screening length calculated from the counterion density only, which is 150 Å for a typical sample ($\Phi=1\%$, $\Gamma=4\%$). Since we are dealing with an isotropic fluid consisting of spherically symmetric aggregates, the scattered intensity can be written

$$I(q)=\frac{N_{\rm ves}}{V}\,S(q)P^{\rm ves}_{\rm step/Gauss}(R,q), \tag{6a}$$

where $N_{\rm ves}/V$ is the number of vesicles per unit volume, $S(q)$ is the structure factor and $P^{\rm ves}_{\rm step/Gauss}(R,q)$ is the form factor which may include polydispersity. This last equation (6a) holds for sufficiently monodisperse size distributions at low volume fractions, where the correlations between position and size—large vesicles surrounded by smaller ones—are negligible. Strictly speaking, the factorization is only possible in the case of a perfectly monodisperse distribution of hard spherical objects. As soon as polydispersity comes in, the measured structure factor obtained by inverting Eq. (6a)

$$S(q)\propto I(q)/\overline{P(q)}, \tag{6b}$$

—where $P(q)$ is an average form factor—is not a purely statistical mechanical quantity any more, as it has been shown by Klein and D'Aguanno [29]. However, as has been pointed out, e.g., by Belloni [30], the measured structure factor $S(q)$ can be reasonably well described as a statistical mechanical quantity for low volume fractions: it is then the Fourier transform of the pair correlation function obtained from the Ornstein-Zernike equation (plus closure relation).

The use of the MSA closure, together with the renormalization by Hansen and Hayter, has proven to give a satisfactory description of the scattered intensity for various charged ''soft'' objects (micelles, vesicles, . . .) [31,32].

We further suppose that vesicle-vesicle interactions will have no impact on the form of the vesicle, nor on the distribution of surfactant within the bilayer. This seems reasonable as we are in a very dilute regime, where intervesicle distances are a lot bigger than vesicle radii. For instance, a simple estimation (using the Yukawa potentiel, cf. [24]) of the electrostatic interaction energy of vesicles carrying 30 elementary charges, of a mean radius of 70 Å at a concentration of $\Phi=1.0\%$ (thus at a average distance of 560 Å) in water yields 0.25 k_BT per vesicle pair. This interaction has important consequences on the average position of vesicles in solution, but it is negligible with respect to a typical deformation energy of the vesicle, which is in a first order approximation $8\pi\tilde{k}\approx 75\,k_BT$.

3. Polydispersity and smearing

Polydispersity in size can be introduced assuming a Gaussian size distribution

$$\frac{1}{\sqrt{2\pi}\Delta_R}\exp\left(-\frac{(R-r)^2}{2\Delta_R^2}\right), \tag{7}$$

where r is the mean radius of the distribution and $(2\Delta_R)/R$ the polydispersity, by appropriate convolution of the form factors $P^{\rm ves}_{\rm step/Gauss}(R,q)$. Note that this simple procedure neglects shape fluctuations at constant size and the polydispersity as derived from such fits can therefore only be seen as an indicative value. Similarly, we take into account the Gaussian distribution of wavelengths of the incident neutrons

$$\frac{1}{\sqrt{2\pi}\Delta_\lambda}\exp\left(-\frac{(\lambda-\lambda_m)^2}{2\Delta_\lambda^2}\right), \tag{8}$$

following the procedure given, e.g., in Ref. [33]. The wavelength spread $(2\Delta_\lambda)/\lambda_m$ of the order of 10% is due to the mechanical wavelength selector geometry. We suppose that this effect dominates collimation effects and intensity smoothing related to the limited spatial resolution of the detector elements, which is true at least in the intermediate and high-q ranges.

4. Results

A typical fit of the scattering pattern obtained in the vesicle phase is shown in Figs. 2 and 3, where two different representations have been used: Fig. 2 shows $I(q)$ versus q

TABLE I. Mean radius R and polydispersity $(2\Delta_R)/R$ of microvesicles as a function of charge Γ with $\Phi=1\%$ and $\Omega=0.5$, no salt.

Charge Γ	$\Gamma=1\%$	$\Gamma=1.5\%$	$\Gamma=2\%$	$\Gamma=3\%$	$\Gamma=4\%$	$\Gamma=5\%$	$\Gamma=7\%$
R (Å)	151±5	122±5	99±5	71±5	56±5	50±5	42±5
$\frac{2\Delta_R}{R}$	>50%	40%	35%	31%	28%	30%	35%

TABLE II. Mean radius R and polydispersity $(2\Delta_R)/R$ of microvesicles as a function of concentration Φ with $\Gamma = 5\%$ and $\Omega = 0.6$, no salt.

Concentration Φ	$\Phi = 0.3\%$	$\Phi = 0.6\%$	$\Phi = 0.9\%$	$\Phi = 1.2\%$	$\Phi = 1.5\%$
R (Å)	34 ± 5	45 ± 5	53 ± 5	58 ± 5	66 ± 5
$\frac{2\Delta_R}{R}$	60%	30%	30%	30%	30%

(full circles), whereas Fig. 3 displays $q^2 I(q)$ versus q, a representation appropriate for bilayer structures (full circles). The sample characteristics are $\Phi = 1\%$, $\Omega = 0.5$, and $\Gamma = 4\%$. The full line corresponds to a fit using Eqs. (6a), (7), and (8) in combination with the Gaussian vesicle form factor, Eq. (4). The Gaussian wavelength spread is $(2\Delta_\lambda)/\lambda_m = 10\%$ and the polydispersity in size of the microvesicles is $(2\Delta_R)/R = 28\%$. The position $q_o = 0.015$ Å^{-1} of the peak of the structure factor $S(q)$ is well reproduced by the Hansen-Hayter-Penfold analytic structure factor, provided that the effective charge of the vesicle has taken 38 elementary charges. This fitted value has to be compared to the total number of charged monomers in the bilayer which is approximately 80 in this particular case. One reason for the discrepancy is the shielding of charges due to counterions inside the vesicle. Another is that we are in a situation where the fully nonlinear Poisson-Boltzmann equation has to be used, and that the Hansen-Hayter-Penfold analytical structure factor relies on a Debye-Hückel-type potential. Considering the level of approximation, the fitted value of the effective charge seems reasonable. The position of the peak of the structure factor can be traced back to the size of the aggregates, since the concentration Φ is known. This provides an additional check of the aggregate geometry, and coincides well, as we have shown in [23]. Additional information about the average size is contained in the absolute intensity scale used. The most important check of the vesicle structural parameters is, of course, given by the form factor. The oscillations in the high-q part of the scattered intensity can easily be shown to be inconsistent with the form factor of a full sphere (globular micelles), and they clearly envelop the form factor of a flat bilayer. The two models proposed, i.e., on the one side the Gaussian profile representing a nonuniform hydration of the polyoxyethylene headgroups of Triton X-100, or, on the other side, the single step profile, both reproduce the form factor reasonably well. In addition to that, we repeated all fits with and without size polydispersity, in order to check the influence of the choice of a Gaussian size distribution function. The radii obtained from all type of fits are close to each other, so we conclude for the sample of Fig. 2 that the mean radius of the vesicles is $R = 56 \pm 5$ Å.

We have performed series of similar experiments, varying the cosurfactant-to-surfactant ratio Ω, the charge Γ, the concentration Φ, and the salinity. The relatively large range of parameters explored experimentally will allow a check of the results of the model presented in the theoretical section. The fitting procedure has been automatized, and all fits resemble, in essence, the fit presented in Fig. 2.

Table I lists the average radius R of microvesicles as a function of charge (Γ), keeping the total amphiphile concentration $\Phi = 1\%$, and the cosurfactant-to-surfactant ratio $\Omega = 0.5$ constant. This result is also drawn in Fig. 7. We observe a monotonic decrease of the vesicle radius with increasing charge, down to very small radii. At high charge ($\Gamma > 5\%$), the scattered intensities still show the characteristic oscillations of the vesicle form factor. Satisfactory fits in terms of vesicles only, however, cannot be obtained any more, and we conclude that smaller objects, presumably micelles, coexist with the vesicles in solution.

In Table II (and also Fig. 8) we report the evolution of the mean radius with concentration (at $\Omega = 0.6$ and $\Gamma = 5\%$ fixed). Microvesicles exist only in a rather narrow dilution range. Nevertheless, a systematic increase in size with increasing concentration is clearly seen. Actually, our electrostatic model (see theoretical section) indeed reproduces this size increase with concentration. We stress the fact that the scattering pattern of even the very small vesicles at $\Phi = 0.3\%$ shows the characteristic form factor oscillations with the high-q asymptotic behavior corresponding to the local bilayer structure. Moreover, the scattering pattern of full spheres (globular micelles) only is again inconsistent with the data.

Table III (and also Fig. 10) finally gives the mean radius as a function of salinity, again starting from a typical vesicle sample ($\Phi = 1\%$, $\Omega = 0.6$, $\Gamma = 5\%$). As expected, the screening effect due to the salt leads to an increase of the vesicle size. The quite surprising instability of the vesicular phase with respect to salt—the sample at 0.5 mM NaCl is in the two-phase region—underlines that the electrostatic effect is crucial.

TABLE III. Mean radius R and polydispersity $(2\Delta_R)/R$ of microvesicles as a function of salinity for ($\Phi = 1\%$, $\Gamma = 5\%$, $\Omega = 0.6$).

Salinity	0 mM	0.1 mM	0.2 mM	0.3 mM	0.4 mM
R (Å)	55 ± 5	55 ± 5	61 ± 5	61 ± 5	68 ± 5
$\frac{2\Delta_R}{R}$	28%	29%	30%	34%	36%

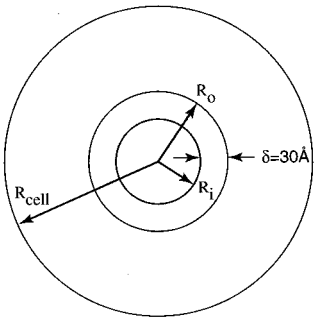

FIG. 5. Vesicle cell model (see text for details).

THEORETICAL SECTION

In the experimental section, we have investigated a thermodynamically stable phase of microvesicles. They exist only in very dilute solutions, at low salinity and moderate charges. At too high concentrations or too high salinity, the system prefers rearranging itself into a swollen lamellar phase. A systematic dependence of the average radius on the total charge can be observed. The aim of this theoretical section is to describe the gas of electrostatically charged vesicles and to derive the size distribution $N(R)dR$, which gives the number density of vesicles of radius between R and $R+dR$. From this distribution $N(R)$, one can derive the average radius and its polydispersity in size, and so check the model against the size measurement.

A. Dominant contributions

Our model includes three contributions. (i) Keeping in mind the strong dependence of the vesicle radius on charge, we suppose that the *electrostatic contribution* [34] to the free energy is crucial. Given the finite concentration of the samples, vesicle-vesicle interactions are not negligible, and the ionic cloud of a given vesicle is confined by the presence of the clouds of surrounding vesicles. We therefore apply a simple thermodynamic cell model [35]. Space is divided up into cells of the same spherical symmetry as the vesicles. Each cell contains one vesicle as well as its co- and counterions. The size of the cell is chosen such that the concentration of each species in a cell equals its global value. The electrostatic contribution to the free energy is then calculated for such a cell. (ii) The *intrinsic bending elasticity* of the neutral bilayer due to molecular packing has to be included. This contribution keeps vesicles from complete electrostatic collapse, and we use the Hamiltonian [Eq. (1)] with an effective bending elasticity constant $\tilde{\kappa}_{\rm eff}=\kappa_{\rm eff}+\overline{\kappa_{\rm eff}}/2$ as a first order approximation. The intrinsic part of the bending energy of a spherical vesicle is then $8\pi\tilde{\kappa}_{\rm eff}$. (iii) We include the mixing entropy of an ideal gas as an estimate of the *translational entropy* of the microvesicles.

B. Cell model

The model, see Fig. 5, is built up and quantitatively specified so as to realistically represent the experimental situations reported above. The bilayer thickness is fixed at $\delta=R_o-R_i=30$ Å, as derived from the swelling behavior of the lamellar phase. The experimental parameters (concentration Φ, cosurfactant to surfactant ratio Ω, charge Γ, and salinity) are translated in terms of the aggregation number N_a of a vesicle of mean radius $R=(R_i+R_o)/2$. The total amount of CPCl dopant is also translated in terms of the number of positive charges N in the bilayer of the vesicle and of the number of positive (N_+) and negative (N_-) ions in solution, with $N_-=N+N_+$ due to charge neutrality. All these charges are confined in the cell of radius $R_{\rm cell}$

$$R_{\rm cell}=\left(\frac{R_o^3-R_i^3}{\Phi}\right)^{1/3}, \tag{9}$$

such that the amphiphile concentration in the cell is equal to Φ. The model allows for different counterion concentrations inside $\{\alpha N_-$ counterions$\}$ and outside $\{(1-\alpha)N_-$ counterions$\}$ the vesicle, for different coion concentrations $[\beta N_+$ and $(1-\beta)N_+$, respectively$]$, and for different surface charge densities at the inner and outer monolayers

$$\sigma_i=\frac{\gamma Ne}{4\pi R_i^2}, \tag{10a}$$

$$\sigma_o=\frac{(1-\gamma)Ne}{4\pi R_o^2}, \tag{10b}$$

where e is the charge of the proton, and α,β,γ are all comprised between 0 and 1. For the evaluation of the entropy of mixing of the ions in the monolayers, we estimate the number of sites of each monolayer. The curvature effect comes into play by offering a different number of sites S_i and S_o for charges on the inner and outer monolayer, respectively,

$$S_i=N_a\frac{R_i^2}{R_i^2+R_o^2}, \tag{11a}$$

$$S_o=N_a\frac{R_o^2}{R_i^2+R_o^2}. \tag{11b}$$

The fraction of sites occupied by the charged species is then given by

$$\varphi_i=\frac{\gamma N}{S_i}, \tag{12a}$$

$$\varphi_o=\frac{(1-\gamma)N}{S_o}. \tag{12b}$$

According to Gauss's theorem, the distribution of charges parametrized by (α,β,γ) sets up the boundary conditions for the radial component of the electric field E (all other components are zero for symmetry reasons) at the inner radius R_i, at the outer radius R_o and at the boundary of the cell $R_{\rm cell}$

$$E(R_i)=\frac{e}{4\pi\varepsilon\varepsilon_o R_i^2}(\alpha N_- -\beta N_+), \tag{13a}$$

$$E(R_o)=\frac{e}{4\pi\varepsilon\varepsilon_o R_o^2}(\alpha N_- -\beta N_+ -N), \tag{13b}$$

$$E(R_{\rm cell})=0. \tag{13c}$$

One then integrates the PB equation for monovalent ions

$$\Delta\psi(\vec{r})=-\frac{e}{\varepsilon\varepsilon_o}\left[n_+^o\exp\left(-\frac{e\psi(\vec{r})}{k_BT}\right)-n_-^o\exp\left(\frac{e\psi(\vec{r})}{k_BT}\right)\right], \tag{14}$$

where ε_o is the vacuum electric permittivity, ε is the dielectric constant of water, Ψ the electric potential, k_B the Boltzmann constant, and n_+^o and n_-^o are the co- and counterion densities at zero potential. This integration in spherical symmetry has to be done numerically, and the result is the electric potential $\Psi(r)$ and, using the Boltzmann equation, the spatial distribution of charges $n_+(r)$ and $n_-(r)$ everywhere in the cell (see the Appendix and Ref. [36] for details).

1. Free energy of a single vesicle in a cell

The electrostatic excess bulk free energy per vesicle cell $F_1^{\rm ves}$ can be written as the sum of an electric energy term proportional to the square of the electric field E and an entropy term (using an ideal gas approximation) accounting for the translational entropy of the ions [35]. It depends on the experimental parameters (Φ, Ω, Γ, salinity), on the distribution of charges (α,β,γ) chosen, and on the mean radius of the vesicle R. We decompose into the contributions of the co- and counterions in the solution surrounding the vesicle $F^{\rm sol}$, and of the charges in the bilayer $F^{\rm bil}$. For a given set of experimental parameters we can write

$$F_1^{\rm ves}(\alpha,\beta,\gamma,R)=F_{\rm el}^{\rm sol}+F_{\rm ent}^{\rm sol}+F_{\rm el}^{\rm bil}+F_{\rm ent}^{\rm bil}. \tag{15}$$

The energy arising from the electric field is

$$F_{\rm el}=\frac{\varepsilon\varepsilon_o}{2}\int|\nabla\psi(\vec{r})|^2d^3r, \tag{16}$$

where the integration has to be carried out over the volume of interest (aqueous solvent or bilayer), and ε is the dielectric constant in that medium. The contributions of the bilayer to $F_{\rm el}$ is

$$F_{\rm el}^{\rm bil}=\frac{e^2[(\alpha-\beta)N_++(\alpha-\gamma)N]^2}{8\pi\varepsilon_{\rm oil}\varepsilon_o}\left(\frac{1}{R_i}-\frac{1}{R_o}\right), \tag{17}$$

where $\varepsilon_{\rm oil}$ is the dielectric constant of the bilayer. The general expression for the entropy of an ideal gas of ions in solution is given by [37]

$$F_{\rm ent}^{\rm sol}=k_BT\int\left[n_+(\vec{r})\ln\left(\frac{n_+(\vec{r})}{\overline{n_+}}\right)+n_-(\vec{r})\ln\left(\frac{n_-(\vec{r})}{\overline{n_-}}\right)-[n_+(\vec{r})+n_-(\vec{r})-\overline{n_+}-\overline{n_-}]\right]d^3r. \tag{18}$$

Equation (18) gives the entropic contribution to the excess free energy compared to a homogeneous distribution of the ions with densities $\overline{n_+}$ and $\overline{n_-}$. We choose $\overline{n_+}$ and $\overline{n_-}$ to be the mean densities of each ionic species, which removes the linear terms in Eq. (18). In the case of the ions in the bilayer, we decompose into the contributions of the two monolayers, and use the usual expression for the ideal entropy of mixing of two species in a monolayer

$$F_{\rm ent}^{\rm bil}=F_{\rm ent}^i+F_{\rm ent}^o, \tag{19a}$$

$$F_{\rm ent}^i=k_BTS_i[\varphi_i\ln(\varphi_i)+(1-\varphi_i)\ln(1-\varphi_i)], \tag{19b}$$

$$F_{\rm ent}^o=k_BTS_o[\varphi_o\ln(\varphi_o)+(1-\varphi_o)\ln(1-\varphi_o)]. \tag{19c}$$

In a given experimental configuration (Φ, Ω, Γ, salinity), the electrostatic free energy per vesicle $F_1^{\rm ves}(R)$ is found by minimizing expression (15) with respect to α, β, and γ.

2. Free energy of an ensemble of vesicles

Defining the $N(R)\,dR$ as the number of vesicles of mean radius between R and $R+dR$ per unit volume, we can calculate the free energy per unit volume due to the ions and counterions in each vesicle of mean radius R

$$F_{\rm ions}^{\rm ves}=\int_{\delta/2}^{\infty}F_1^{\rm ves}(R)N(R)dR. \tag{20}$$

In addition to that, we include an ideal gas entropy as an approximation for the translational entropy of the vesicles

$$F_{\rm ent}^{\rm ves}=k_BT\int_{\delta/2}^{\infty}N(R)\left[\ln\left(\frac{N(R)}{N_o}\right)-1\right]dR, \tag{21}$$

where $N_o\,dR$ is a fixed reference vesicle density. With the volume $V(R)$ of surfactant in a vesicle of radius R, the conservation of the total surfactant volume (volume fraction Φ) can be written as

$$\int_{\delta/2}^{\infty}V(R)N(R)dR=\Phi. \tag{22}$$

This constraint can be fullfilled by including a Lagrange multiplier μ in the total energy minimization. The grand potential of the ensemble $\Phi_{\rm tot}$, with the intrinsic elastic bending energy contribution per vesicle of $8\pi\tilde{\kappa}_{\rm eff}$, then reads

$$\Phi_{\rm tot}[\mu,T,N(R)]=\int_{\delta/2}^{\infty}[F_1^{\rm ves}(R)+8\pi\tilde{\kappa}_{\rm eff}]N(R)dR+F_{\rm ent}^{\rm ves}-\mu\int_{\delta/2}^{\infty}V(R)N(R)dR. \tag{23}$$

Its minimization with respect to $N(R)$ yields

$$N(R)=N_o\exp\left(\frac{-[F_1^{\rm ves}(R)+8\pi\tilde{\kappa}_{\rm eff}-\mu V(R)]}{k_BT}\right)=N_o\exp\left(\frac{-g(R)}{k_BT}\right). \tag{24}$$

From $N(R)$, we can then derive the mean radius and the polydispersity in size.

C. Results

Using the calculations described above, the electrostatic free energy per ion and the mean radius of the vesicles can

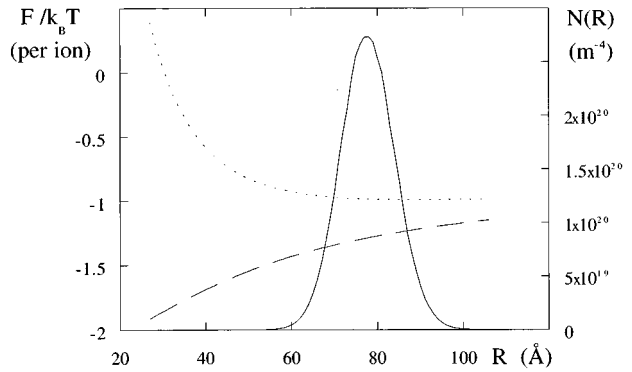

FIG. 6. Typical model result: Electrostatic excess free energy per ion (broken line); electrostatic excess free energy per ion plus intrinsic bending elasticity contribution $\tilde{\kappa}_{\text{eff}}=3k_BT$ (dotted line); size distribution function $N(R)$ (full line) for $\Phi=1\%$, $\Omega=0.5$, $\Gamma=3\%$, no salt.

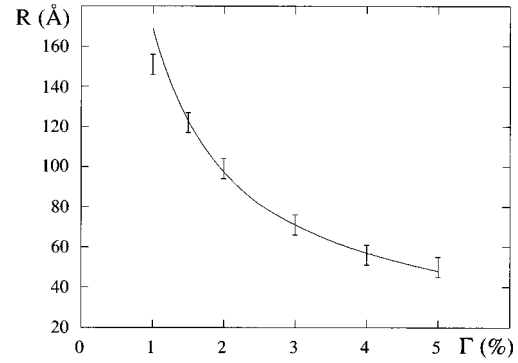

FIG. 7. Comparison of experiment (with error bars) and model results ($\tilde{\kappa}_{\text{eff}}=2.7\pm0.2k_BT$): mean vesicle radius as a function of charge Γ for $\Omega=0.5$, $\Phi=1\%$; no salt.

be calculated for arbitrary vesicle parameters (charge, concentration, bilayer width, etc). In Fig. 6 we report on a typical result. The broken line represents the electrostatic free energy due to ions and counterions in vesicular geometry as a function of mean vesicle radius R and in units of k_BT per ion, according to Eq. (15). It is a monotonically increasing function of R, which indicates that the electrostatic contributions alone would favor a complete collapse of the vesicle. Adding to this free energy the intrinsic bending elasticity contribution of $8\pi\tilde{\kappa}_{\text{eff}}$, we obtain the dotted line. As expected, forming very small vesicles is now energetically penalized, and vesicles will adopt some equilibrium radius. Using Eq. (24), we determine the size distribution $N(R)\,dR$, which gives the number of vesicles per unit volume of average radius R (full line). This size distribution function is symmetric about its most probable value, and the average radius and its polydispersity in size (full width at half maximum/average radius) can be easily deduced.

For comparison with the experimental results listed in Tables I–III, we calculated the average radius, polydispersity, and free energy per unit volume expected for a concentration of $\Phi=1\%$, a cosurfactant to surfactant ratio of $\Omega=0.5$, a bilayer width of $\delta=30$ Å, and charges ranging from $\Gamma=1\%-5\%$. The intrinsic contribution to the bending energy—$8\pi\tilde{\kappa}_{\text{eff}}$ per vesicle—is included. Fitting the theoretical mean radius to the mean radius obtained from small angle neutron scattering (SANS) yields $\tilde{\kappa}_{\text{eff}}=2.7\pm0.2\,k_BT$, which is a reasonable order of magnitude for surfactant bilayer systems (typically in the range $0.5-5\,k_BT$ according to current literature). The result—the mean radius R of the vesicle as a function of charge Γ—is plotted in Fig. 7 (full line). The experimental values for R are superimposed (with error bars). The theoretical polydispersity is about 15%, which is somewhat less than what we observe experimentally.

The experimental dependence of the mean vesicle radius R on concentration Φ is documented in Table II of the experimental section. This effect is due to the confinement of the counterions into smaller volumes, and should be reproduced by the cell model which defines the volume accessible to the ionic cloud. In Fig. 8 we plot the mean radius of the microvesicles as a function of concentration Φ (with error bars, see Table II), and superimpose the theoretical result (full line). Fitting $\tilde{\kappa}_{\text{eff}}$ yields $2.9\pm0.2\,k_BT$.

In the experiment, as can be seen in the phase diagram (Fig. 1), the vesicles are unstable with respect to increasing concentration. A two-phase region separates highly curved objects (the microvesicles) from flat or weakly curved mesostructures (lamellar phase, exhibiting spontaneous onion textures). The position of the phase boundary depends mainly on the charge Γ, and varies from $\Phi=0.6\%$ at $\Gamma=0.5\%$, to $\Phi=2.5\%$ at $\Gamma=10\%$. In this respect, the electrostatic cell model presents quite a peculiar behavior which deserves comparison with the experiment: upon increasing concentration, it exhibits a first order transition from small to big vesicles. This takes place at a concentration of $\Phi=5.5\%$, which is comparable to the experimental phase transition. $g(R)$ at the transition [Eq. (24)] is plotted in Fig. 9. Of course the model cannot reproduce the formation of smectic onions since the geometry of the objects is fixed to unilamellar vesicles. Nevertheless, we think that the formation of the big vesicle population reveals the higher stability of objects having lower curvature at higher concentration.

Finally, we calculated the evolution of the mean vesicle radius with salinity. As shown in the experimental section, vesicle size should increase with salinity due to electrostatic screening effects. In Fig. 10 we compare the experimental results to our model results, using an effective intrinsic bend-

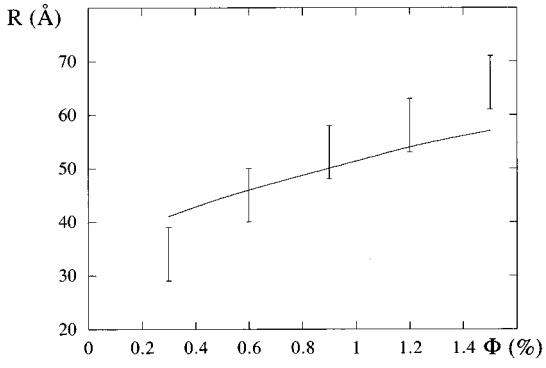

FIG. 8. Comparison of experiment (with errorbars) and model results ($\tilde{\kappa}_{\text{eff}}=2.9\pm0.2k_BT$): mean vesicle radius as a function of concentration Φ for $\Omega=0.6$, $\Gamma=5\%$; no salt.

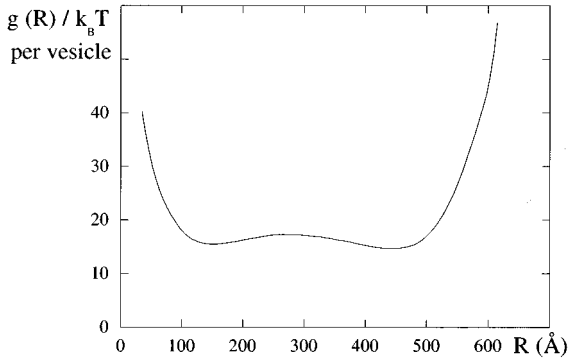

FIG. 9. Small to big vesicle transition: $g(R)$ for $\Phi=5.5\%$, $\Omega=0.6$, $\Gamma=5\%$; no salt using $\tilde{\kappa}_{\text{eff}}=3k_BT$.

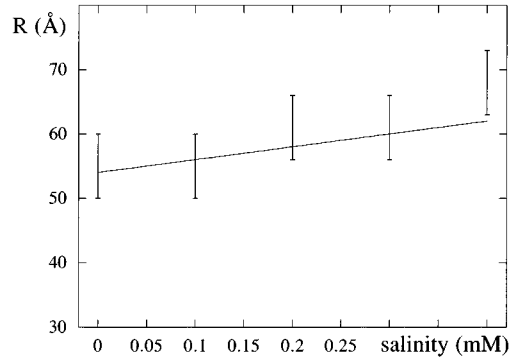

FIG. 10. Comparison of experiment (with errorbars) and model results ($\tilde{\kappa}_{\text{eff}}=3.1\pm0.2k_BT$): mean vesicle radius as a function of salinity for $\Omega=0.6$, $\Gamma=5\%$, $\Phi=1\%$.

ing modulus of $\tilde{\kappa}_{\text{eff}}=3.1\pm0.2k_BT$. We conclude that the model reproduces the tendency of the vesicles to grow with increasing salinity.

CONCLUDING REMARKS

Figures 7, 8, and 10 show that our electrostatic model reproduces experimental (SANS) results corresponding to varying charge densities, concentrations, and salinities fairly well. Its main features are the possibility of the ions to equilibrate across the whole cell according to the Poisson-Boltzmann equation (14) and the approximative treatment of vesicle-vesicle interaction via the confinement of the ions around the vesicle, expressed by a finite cell radius. The model involves only one free parameter, the intrinsic bending elasticity modulus $\tilde{\kappa}_{\text{eff}}$, and its fitted value, a few k_BT, corresponds well to the bending moduli measured in similar mixed (surfactant+cosurfactant) systems: it is known from Ref. [38] that in mixed systems the compositions of the two monolayers readjust upon bending so that the effective rigidity (at relaxed compositions) is lower than that of pure systems.

Deviations of the model predictions from the experimentally observed values occur close to phase transition, e.g., for very small vesicles, where the interpretation of the SANS patterns becomes delicate. One of the reasons for this is the possible coexistence of different populations (vesicle-micelle, or very polydisperse vesicles). Another is the possibly asymmetric distribution of TX100 and octanol, with the inner monolayer richer in octanol and the outer one richer in TX100. The contrast profile is then asymmetric about the mean radius. On the other hand, theoretical limitations are introduced by setting the CPCl dissociation constant to 1, and by the use of ideal gas entropies. In addition to that, introducing the molecular packing requirement in terms of an effective bending constant $\tilde{\kappa}_{\text{eff}}$ may not be reliable at very large curvatures. Including higher order terms into Eq. (1) would make the model too arbitrary. Finally, one could get rid of the free parameter $\tilde{\kappa}_{\text{eff}}$ by working out a detailed microscopic calculation of the intrinsic bending constant, as, e.g., done by May and Ben-Shaul [39]. Bergstöm [40] actually calculated the size distribution of the vesicles observed by Kaler and co-workers: his predictions closely resemble the size distribution determined from electron microscopy. A complete thermodynamic model has been worked out for mixed cationic-anionic vesicles by Yuet and Blankschtein [41]. Such calculations are, nevertheless, very complicated and technical.

The theories of the bending elasticity of charged bilayers (especially Refs. [1] and [2]) proposed for the limiting case $\lambda_{\text{Debye}}\ll R$, where R is a typical dimension characterizing the local curvature, predict a curvature instability for flat isolated membranes at high area charge density. This is consistent with the observation of the replacement of the highly diluted lamellar phase by microvesicles when increasing the area charge density above some critical value. But such theories cannot predict the characteristics of strongly interacting microvesicles at equilibrium. Recently, Daicic *et al.* have proposed a perturbative approach of the Poisson-Boltzmann equation in a spherical cell model [42], where the free energy expansion is translated in terms of effective rigidity constants: this is an interesting attempt to generalize the frame of the effective rigidity to the case of nonisolated vesicles in strong electrostatic interaction. But this is still a perturbation approach (about the flat state), which in essence is not appropriate for very high curvatures and large screening lengths, as it is the case of microvesicles. In order to model these, we had to work out numerical calculations, solving the Poisson-Boltzmann equation for arbitrary curvatures and screening lengths. A further essential ingredient of our model is that it allows for a nonsymmetrical distribution of the charges in the inner and the outer monolayer of the vesicles and that the co- and counterions can equilibrate across the whole cell (inside and outside the vesicle). We worked out alternative simulations where these internal degrees of freedom were frozen: the predictions obtained are different which means that the internal degrees of freedom have quantitatively important effects.

In conclusion, we have measured the evolution of the size of the microvesicles with all relevant parameters from neutron scattering: the data treatment exploits altogether the form factor of the individual vesicles and the interference factor arising from correlations in the positions of their center of mass. In order to interpret such accurate size measurements, we construct a cell model and solve the Poisson-

Boltzmann equation in the cell: this model is found to agree well with the scattering data. However, due to the spherical symmetry of the cell, the model has to be solved numerically: although the agreement is good, it is difficult in these conditions to understand qualitatively what particular effect is at the origin of the instability of flat bilayers in favor of small highly curved vesicles. A possible explanation might be the following. The entropy of the counterions strongly favors the dissociations of infinite bilayer into smaller subunits which allow for a more homogeneous distribution of the counterions in space. In this respect, microvesicles are favorable since they represent the smallest aggregates compatible with an association of the surfactant molecules in bilayers. As a matter of fact, in absence of an intrinsic rigidity $\tilde{\kappa}_{\mathrm{eff}}$, the model would predict a complete collapse of the vesicles. However, this explanation fails when concentration increases since, very soon, the microvesicles phase separate with the onion phase (above typically 3% concentration). Interestingly, the model predicts as well a ''first order'' transition to large sizes in the same range. But, up to now, we did not succeed in making sense of this transition from simple intuitive arguments.

ACKNOWLEDGMENTS

We would like to thank Christian Ligoure for helpful discussions.

APPENDIX: NUMERICAL INTEGRATION

The numerical integration of the PB equation [Eq. (14)] is done using a fourth order Runge-Kutta adaptive step size algorithm. In the case of counterions only, n_-^0 is the natural parameter that has to be varied to fulfill the boundary conditions, e.g., with a Newton-Raphson algorithm. In the presence of co- and counterions, numerical divergences of the electric potential are more difficult to avoid than in the counterion only case. We therefore switched to a hypothetical salt reservoir description, which amounts to putting $n_+^0 = n_-^0 = n^o$ and vary n^o and the value of the potential at the cell boundary Ψ_0 instead of n_+^0 and n_-^0 in order to fulfill the boundary conditions. n^o being an averaged value, this pair of variables is somewhat more intuitive. The problem of the minimization of the electrostatic free energy as a function of α,β,γ is solved in two steps. For a given (α,β) pair, the minimum, with respect to γ, can be found rapidly, as only an evaluation of Eqs. (17) and (19) is necessary. The minimum with respect to α and β can be evaluated by a steepest descent search, as the surface $F_1^{\mathrm{ves}}(\alpha,\beta)$ is smooth.

An estimate of numerical errors is obtained by comparing the volume integral over the numerically found co- and counterion densities to the number of charges actually needed to reach electroneutrality. These relative errors are kept to less than 10^{-4} for all the results presented in this article.

[1] H. N. W. Lekkerkerker, Physica A **159**, 319 (1989).
[2] D. J. Mitchell and B. W. Ninham, Langmuir **5**, 1121 (1989).
[3] M. Winterhalter and W. Helfrich, J. Phys. Chem. **92**, 6865 (1988).
[4] M. Winterhalter and W. Helfrich, J. Phys. Chem. **96**, 327 (1992).
[5] A. Fogden and B. W. Ninham, Langmuir **7**, 590 (1991).
[6] P. Pincus, J. F. Joanny, and D. Andelman, Europhys. Lett. **11**, 763 (1990).
[7] J. L. Harden, C. Marques, and J. F. Joanny, Langmuir **8**, 1170 (1992).
[8] P. G. Higgs and J. F. Joanny, J. Phys. (France) **51**, 2307 (1990).
[9] V. Kumaran, J. Chem. Phys. **99**, 5490 (1993).
[10] C. Ligoure and G. Porte, J. Chem. Phys. **102**, 4290 (1995).
[11] W. Helfrich, Z. Naturforsch. C **28**, 693 (1973).
[12] H. Hoffmann, C. Thunig, P. Schmiedel, and U. Munkert, Langmuir **10**, 3972 (1994).
[13] H. Hoffmann, U. Munkert, C. Thunig, and M. Valiente, J. Colloid Interface Sci. **163**, 217 (1994).
[14] C. Thunig, G. Platz, and H. Hoffmann (unpublished).
[15] J. Wuertz and H. Hoffmann, J. Colloid Interface Sci. **175**, 304 (1995).
[16] S. Ristori, J. Appell, and G. Porte, Langmuir **12**, 686 (1996).
[17] P. Hervé, D. Roux, A. M. Bellocq, F. Nallet, and T. Gulik-Krzywicki, J. Phys. (France) II **3**, 1255 (1993).
[18] L. L. Brasher, K. L. Herrington, and E. W. Kaler, Langmuir **11**, 4267 (1995).
[19] E. W. Kaler, A. K. Murthy, B. Rodriguez, and J. A. N. Zasadzinski, Science **245**, 1371 (1989).
[20] E. W. Kaler, K. L. Herrington, A. K. Murthy, and J. A. N. Zasadzinski, J. Phys. Chem. **96**, 6698 (1992).
[21] R. Schomäcker and R. Strey, J. Phys. Chem. **98**, 3908 (1994).
[22] E. Z. Radlinska, T. N. Zemb, J. P. Dalbiez, and B. W. Ninham, Langmuir **9**, 2844 (1993).
[23] J. Oberdisse, C. Couve, J. Appell, J. F. Berret, C. Ligoure, and G. Porte, Langmuir **12**, 1212 (1996).
[24] J. B. Hayter and J. Penfold, Mol. Phys. **42**, 109 (1981); J. P. Hansen and J. B. Hayter, *ibid.* **46**, 651 (1982).
[25] D. C. Morse and S. T. Milner, Europhys. Lett. **26**, 565 (1994).
[26] B. D. Simons and M. E. Cates, J. Phys. (France) II **2**, 1439 (1991).
[27] M. Mille and G. Vanderkooi, J. Colloid Interface Sci. **61**, 455 (1977).
[28] M. Gradzielski, D. Langevin, L. Magid, and R. Strey, J. Phys. Chem. **99**, 13232 (1995).
[29] R. Klein and B. D'Aguanno, in *Static Light Scattering: Principles and Developments*, edited by W. Brown (Oxford University Press, New York, 1996).
[30] L. Belloni, in *Neutron, X-Ray and Light Scattering*, edited by P. Lindner and Th. Zemb (North-Holland, Amsterdam, 1991), Delta Series.
[31] B. Cabane, R. Duplessix, and Th. Zemb, J. Phys. (France) **46**, 2161 (1985).
[32] E. Z. Radlinska, B. Ninham, J.-P. Dalbiez, and Th. Zemb, Colloids Sur. **46**, 213 (1990).
[33] G. A. McConnell, M. Y. Lin, and A. P. Gast, Macromolecules **28**, 6754 (1995).
[34] E. J. W. Verwey and J. T. G. Overbeek, *Theory of Stability of Lyophobic Colloids* (Elsevier, New York, 1948).

[35] R. A. Marcus, J. Chem. Phys. **23**, 1057 (1955).
[36] M. Dubois, Th. Zemb, L. Belloni, A. Delville, P. Levitz, and R. Setton, J. Chem. Phys. **96**, 2278 (1992).
[37] D. Andelman, in *Handbook of Physics of Biological Systems* (Elsevier Science, New York, 1989), Vol. 1.
[38] S. A. Safran, P. A. Pincus, D. Andelmann, and F. C. MacIntosh, Phys. Rev. A **43**, 1071 (1991).
[39] S. May and A. Ben-Shaul, J. Chem. Phys. **103**, 3839 (1995).
[40] M. Bergström, Langmuir **12**, 2454 (1996).
[41] P. K. Yuet and D. Blankschtein, Langmuir **12**, 3802 (1996).
[42] J. Daicic, A. Fogden, I. Carlsson, H. Wennerström, and B. Jönsson, Phys. Rev. E **54**, 3984 (1996).